Axial Proton Probing of Magnetic and Electric Fields Inside Laser-Driven Coils

J. L. Peebles, J. R. Davies, D. H. Barnak, T. Cracium, M. J. Bonino, and R. Betti

Laboratory for Laser Energetics, University of Rochester

The capability of generating strong, localized, and applicable magnetic fields provides an excellent opportunity in high-energy-density (HED) research environments. Such a tool would have applications in magnetizing HED plasmas,[1,2] field compression leading to fusion yield enhancement,[3–7] particle collimation,[8,9] and magnetized shock physics.[10–14] The laser-driven coil (LDC) has been proposed several times in previous decades[15–27] as a method to generate kilotesla (kT) magnitude fields in a small volume, with the precision of a laser system. Fields ranging from 0.001 T (Ref. 20) to over 1 kT (Ref. 15) have been inferred from previous experiments. Since the generation of these fields can be precisely tuned using the geometry of a thin metal target, LDC's can potentially provide a substantial benefit over traditional pulsed-power, magnetic-field–generation mechanisms[28,29] because they are easier to place in close proximity to experiments and are "triggered" precisely by a laser. LDC's usually consist of two parallel plates connected with a wire loop advantageously shaped to generate a field. A laser passes through a hole in one of the plates and ejects hot electrons from one plate to the other. The charge displacement then draws a return current through the loop from the source plate on the other side, which may also become negatively charged after capturing some electrons from the interaction.[15–27]

Axial Proton Probing and Motivation

The method for diagnosing fields inside the region of interest of an LDC in this summary is "axial proton probing." High-energy protons travel axially through the loop rather than transversely. Since magnetic-field lines must always form a closed loop, a significant axial field will generate a radial field. This radial field will induce a deflection of protons traveling in the axial direction. Upon initial inspection, it would appear that the protons should not see any net deflection at all from a radial field; any deflection of a proton incurred by the radial field will be reversed upon encountering the opposing radial field when leaving the coil. This approximation only holds true, however, in the paraxial approximation. In reality, a proton will be deflected significantly by the initial field, leading to a rotation as it passes through the coil. It will then be returned (approximately) to its original velocity vector after leaving, resulting in a measurable rotational shift as seen in the synthetic radiograph in Fig. 1(a). There are also two second-order effects: the field encountered by the exiting proton is not necessarily the opposite of the field it encountered when it entered and the velocity vector of the proton leaving is not identical to when it entered. Therefore, in theory, a magnetic field generated by a current traveling in the loop will induce a rotation in the proton image when using a spatial fiducial. The estimated mesh rotation, calculated from multiple simulated loops with only a magnetic field, is described by Eq. (1):

$$\theta^{\circ}_{\mathrm{rot}} \approx \frac{0.23 I_{\mathrm{loop}} r^{-0.27}}{\sqrt{E_{\mathrm{p}}}}, \tag{1}$$

where r is the radius of the loop, I_{loop} is the current, and the deflection depends inversely on the square root of the proton energy E_{p}, as expected. The anticipated deflection of protons due to the expected electric field is shown in Fig. 1(b), which shows a clear focusing and stretching effect on the mesh fiducial. The clear difference in the deflection effect demonstrates that this method of proton radiography is able to distinguish deflection contributions from radial electric and magnetic fields.

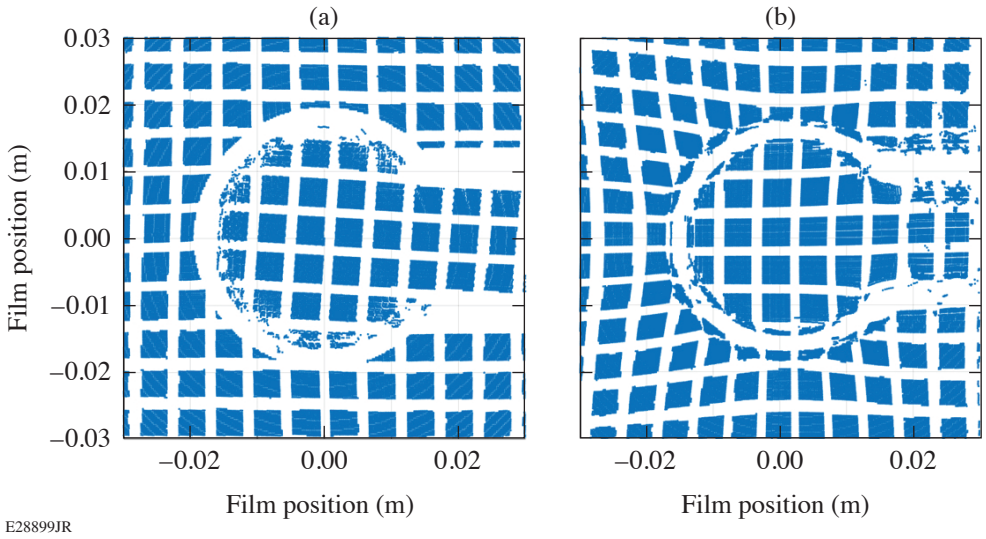

Figure 1
(a) A synthetic axial radiograph (magnification ~16) demonstrates the rotation of the mesh fiducial due to the radial magnetic field. A 90-kA current corresponding to 80 T at the center of the loop was applied along the wire surfaces. (b) A synthetic radiograph demonstrates the pinching of the mesh due to an electric field generated by displacing electrons from the wire.

Axial proton probing also provides more-comprehensive information at the center of the coil regarding plasma density. Any sheath structure, plasma jets, or significant plasma density will be detectable in the axial probe, whereas coil material will always block a transverse probe. Information about conditions inside the coil is of interest for any experiment that would use a LDC to magnetize a target inside of it. Since creating synthetic radiographs for comparison requires several assumptions on location of charge and current, the information of sheath structure position is extremely helpful in reducing parameter space. Since deflections are relatively weaker in the axial proton probing case, more use can be made of the mesh fiducial. Each mesh line and each grid point are effective measurements of the fields in the system, providing hundreds of data points with each shot rather than one or two, as is the case with transverse proton probing.

Experimental Setup

To verify the effectiveness of the axial proton probe, experiments were conducted on the OMEGA EP Laser System. The goal of these experiments was not to generate the field with the highest magnitude, rather it was to generate a field that could be comprehensively diagnosed with the axial probe. Therefore a coil with a comparatively large radius (750 μm) was chosen due to concerns that with high magnitude fields and potential plasma blowoff, protons could be attenuated when passing through the coil. As shown in Fig. 1, an anticipated field of 80 T would result in a modest rotation that would be quantifiable. Furthermore, current along the parallel wires would induce a "twist" across the parallel wires, which could be detected. The experiment had an additional goal of testing a single-plate coil design, similar to experiments performed by Zhu *et al.*[24] The single-plate geometry enhances the feasibility of fielding the LDC as a magnetic-field generator on other experimental platforms such as magnetized inertial confinement fusion and magnetized shocks.

To achieve these goals, experiments were performed with multiple setups and coil types as shown in Fig. 2. Targets consisted of a laser-cut, 2-mm-diam, 0.1-mm-thick copper disk driven by a 1-ns, 1.25-kJ, 351-nm long-pulse beam with a nominal intensity of 6×10^{15} W/cm^2. The disk was attached to a 750-μm-radius coil of the same material via a 2-mm stretch of wire with a 0.1×0.1-mm-sq cross section. The coil would then either return to a second plate placed in front of the first with a 1.2-mm hole placed for the driving beam (double-plate configuration) or connect to a flag with near mass equivalence placed away from the driven plate (single-plate configuration). The double-plate configuration tested two plate separations: 0.5 mm and 0.8 mm. The targets were constructed by cutting a single piece out of a copper foil and then subsequently shaping the target around a custom fixture. The target stalk (made of silicon carbide) was attached to either the flag or the undriven plate in order to remove the stalk as a potential source of electrons.

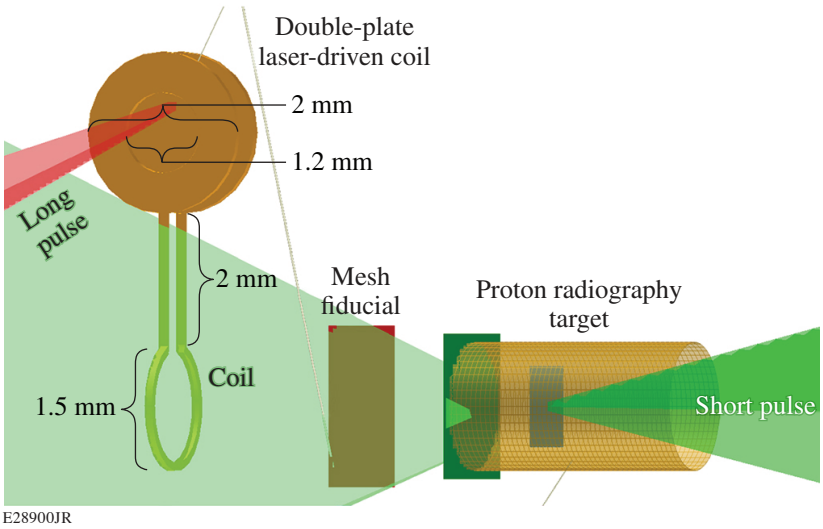

Figure 2
Experimental setup for the double-plate experiments. An OMEGA EP long-pulse beam passes through a front plate and hits the driving plate, which induces a current in the loop. The loop is probed with protons generated by a proton radiography target with a mesh fiducial placed halfway between the source and target.

The coil was probed using a short-pulse–based, proton radiography setup. A 0.7-ps, 300- to 500-J beam, with a nominal intensity of 0.6 to 1 × 10^{20} W/cm^2, was incident on a copper foil placed in a shielded tube 5 mm from the coil. A tantalum shield protected the foil from any potential debris. A copper–rhodium mesh fiducial (100 × 100-μm mesh spacing with 30-μm-thick wire) was placed halfway between the coil and the proton source. Protons with energy up to 40 MeV were accelerated and detected by a radiochromic film stack placed 8 cm away from the coil.

Experimental Results and Comparison to Synthetic Radiographs

Figure 3 shows experimental radiographs using two different proton energies, taken at 1.1 ns, just after the driving laser has turned off. Overlayed in color are synthetic radiographs, which used a combination of electric charge and current distributions to best recreate the experimental image. The double-plate configuration [Figs. 3(a) and 3(b)] with 0.5-mm spacing shows limited twisting distortion of the mesh. Distortions take two primary forms: a general "pull" on the mesh toward the driven plate to the right on the radiograph and radial "spray" emanating from the wire in all directions in the loop. The general pull is most noticeable when comparing the size of mesh grids on the right and the left of each radiograph, where grids on the right are shrunk and focused compared with those on the left. This is consistent with a large electric field that surrounds all target surfaces and increases with proximity to the driven plate. The radiographs also indicate multiple populations of electrons ejected from the wire material. To recreate the features in the synthetic radiographs, *no current distribution is required in the system*. The energy present in the electrostatic field used to create the synthetic radiographs over the entire simulation box was 36 J, or a conversion rate of nearly 3% from the full laser energy.

The single-plate case shows a significant departure in terms of distortion type. The sheath becomes significantly detached from the coil and does not conform to the shape of the wire. An asymmetric distortion can be seen near the parallel wires, where mesh on top of the loop is expanded and mesh on the bottom is squeezed. This indicates that a current is present that would preferentially flow along the sheath on the inside of the loop since the sheath plasma is a good conductor and the shortest path contains the least inductance for the system. Another indication that a significant current is present in the single-plate case is the twisting of the reference mesh near the parallel wires. A simple rotation of the mesh, as was anticipated in Fig. 1, is not obvious, indicating that a significant electrostatic charge is present in the single-plate case as well. The current used in generating the synthetic radiographs is initially 170 kA at the driven wire and decays as it traverses the loop. The total energy in the magnetic field is approximately 37 J, or a conversion efficiency from the laser of 3.0%. The total energy in the electrostatic field for the

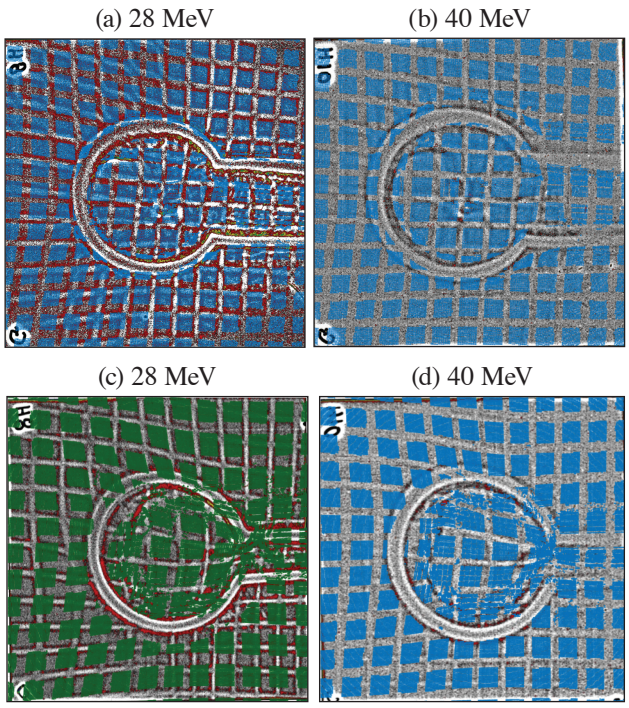

Figure 3
[(a),(b)] Synthetic radiographs created by passing 28- and 40-MeV protons through the fields generated by an electric charge distribution for double-plate experiments. The resulting synthetic radiographs are overlayed on top of the experimental data for comparison. [(c),(d)] A similar treatment for single-plate experiments. A current distribution was required in addition to the charge distribution to reproduce the experimental data in the synthetic radiographs.

simulation box is 20 J, or 1.6% of the incident laser energy. The field is approximately 65 T in the center of the loop; if the current were even throughout the loop, the field would have been much higher at around 140 T.

The proton radiographs from the single-plate experiment indicate that while a current is present, it is in a transient regime for our target design. Angular filter refractometry data and 2-D radiation-hydrodynamic simulations show that radiation ejects electrons from the loop before the current can propagate from the laser-heated region through the connecting solid wire. Therefore, photoelectrons will provide the return current, which allows faster propagation of current than is possible in the unheated copper, consistent with the proton-probing data. Indeed, photoelectrons would be expected to carry the majority of the current since they offer the lowest resistance and lowest inductance path for the current. For our parameters, current propagation in 1.1 ns is observed to be limited to around 3 mm, which is part way around the loop. For most of the other published designs, this would be far enough to drive a current around the entire loop but not far enough to draw any significant current from a second plate. Although current may be present around the entire loop in smaller coils, it could still be nonuniform.

These findings indicate the need to reduce the size of the loop and length of the wire to be as small as possible for LDC's. Doing so creates problems, however, in regard to fielding LDC's in order to magnetize experiments. Reducing the parallel wire length would result in the loop being placed even closer to the driving plate interaction, which would cause more x-ray interference in both the loop and the experiment being magnetized. Placing a shield between the driven plate and magnetized experiment would also prove to be problematic since any x rays will expand material off the shield and cause current to bypass the loop entirely, through the plasma off the shield surface. Reducing the gap between the parallel wires poses a similar problem to the parallel disks, where plasma expansion may simply cause a short circuit. Reducing the loop size removes much of the magnetizing capability of LDC's since loop size determines the size of the system being magnetized. For example, any magnetized inertial fusion concept would require a loop *larger*, not smaller, than the one fielded in our experiments in order to magnetize targets that are typically 1 mm or larger in size.

The data show more potential difficulties for the double-plate–type LDC in addition to those seen with the single plate. First, the driving interaction for the LDC bathes the entire target in x rays, causing significant plasma to form over the entire surface of the LDC. This may be initially beneficial since it will allow current to be drawn more readily, rather than from a cold, solid

material. However, the undriven plate is expanded significantly by these x rays due to its proximity to the interaction. The coil is therefore short circuited very quickly before any meaningful magnetic field is generated. This means that the second plate places an upper limitation on energy and intensity of the driving laser, which depends on the spacing between the plates and material. As plate spacing is increased, the coil's inductance is increased to account for the larger gap. It becomes apparent that increasing the plate spacing to address these issues sufficiently will result in a system that tends toward a single-plate design anyway. Adding the additional plate provides benefit only if electrons can be captured by the second plate and the LDC size is small enough that the charge can meaningfully contribute to the current traveling through the loop. Creating an LDC small enough to benefit from the second plate, however, introduces all of the risks of a small LDC system: short circuiting, x-ray interference, and small magnetized volume.

These findings indicate some design considerations for consistent laser-driven coils. First, a single-plate design should be used with minimal distance between the driving plate and coil; in our experiments current appears to propagate significantly for only 3 mm of coil length. The double-plate design appears to offer little benefit for substantial risk and target complexity. Corners should be removed from the loop; even though, in theory, this would result in a less symmetric field, the corners are prime positions for electric-field enhancement, electron emission, and abnormal sheath formation. The laser driver's pulse length should be increased and intensity decreased in order to provide time for the system to respond.

This material is based upon work supported by U.S. Deparment of Energy (DOE) grant DE-SC0016258 from the Office of Fusion Energy Sciences and by the DOE National Nuclear Security Administration under Award Number DE-NA0003856, the University of Rochester, and the New York State Energy Research and Development Authority.

1. G. Fiksel *et al.*, Phys. Rev. Lett. **113**, 105003 (2014).
2. W. Fox, A. Bhattacharjee, and K. Germaschewski, Phys. Rev. Lett. **106**, 215003 (2011).
3. S. A. Slutz *et al.*, Phys. Plasmas **17**, 056303 (2010).
4. D. H. Barnak *et al.*, Phys. Plasmas **24**, 056310 (2017).
5. J. R. Davies *et al.*, Phys. Plasmas **24**, 062701 (2017).
6. H. Nagatomo *et al.*, Nucl. Fusion **53**, 063018 (2013).
7. H. Cai, S. Zhu, and X. T. He, Phys. Plasmas **20**, 072701 (2013).
8. A. Arefiev, T. Toncian, and G. Fiksel, New J. Phys. **18**, 105011 (2016).
9. T. Johzaki *et al.*, Plasma Phys. Control. Fusion **59**, 014045 (2016).
10. G. Gregori *et al.*, Nature **481**, 480 (2012).
11. J. Meinecke *et al.*, Nat. Phys. **10**, 520 (2014).
12. N. C. Woolsey *et al.*, Phys. Plasmas **8**, 2439 (2001).
13. D. B. Schaeffer *et al.*, Phys. Plasmas **19**, 070702 (2012).
14. D. B. Schaeffer *et al.*, Phys. Plasmas **24**, 041405 (2017).

15. H. Daido *et al.*, Phys. Rev. Lett. **56**, 846 (1986).

16. J. J. Santos *et al.*, New J. Phys. **17**, 083051 (2015).

17. S. Fujioka *et al.*, Sci. Rep. **3**, 1170 (2013).

18. K. F. F. Law *et al.*, Appl. Phys. Lett. **108**, 091104 (2016).

19. C. Courtois *et al.*, J. Appl. Phys. **98**, 054913 (2005).

20. A. Tarifeño, C. Pavez, and L. Soto, J. Phys.: Conf. Ser. **134**, 012048 (2008).

21. L. Gao *et al.*, Phys. Plasmas **23**, 043106 (2016).

22. C. Goyon *et al.*, Phys. Rev. E **95**, 033208 (2017).

23. W. W. Wang *et al.*, Plasma Physics Archive, available at https://arxiv.org/abs/1411.5933v1 (2017).

24. B. J. Zhu *et al.*, Appl. Phys. Lett. **107**, 261903 (2015).

25. K. Matsuo *et al.*, Phys. Rev. E **95**, 053204 (2017).

26. V. V. Korobkin and S. L. Motylev, Sov. Tech. Phys. Lett. **5**, 474 (1979).

27. V. Ivanov *et al.*, Bull. Am. Phys. Soc. **64**, CO8.00008 (2019).

28. G. Fiksel *et al.*, Rev. Sci. Instrum. **86**, 016105 (2015).

29. B. B. Pollock *et al.*, Rev. Sci. Instrum. **77**, 114703 (2006).